Sensors and Materials, Vol. 13, No. 5 (2001) 293–301
MYU Tokyo

S & M 0450

Silicon Etch Anisotropy in Tetra-Methyl Ammonium Hydroxide: Experimental and Modeling Observations

Les M. Landsberger*, Anand Pandy and Mojtaba Kahrizi

Department of Electrical & Computer Engineering,
Concordia University, Montreal, QC, Canada H3G- 1M8

(Received October 1, 2000; accepted December 1, 2000)

Key words: anisotropic etching of silicon, bulk micromachining, crystal facets, TMAH, anisotropy

This work considers wagon-wheel-based under-etch experiments of {110} and {100} silicon in tetra-methyl ammonium hydroxide (TMAH) at 25 wt% and 12 wt% at 80°C. The under-etched surfaces often consist of two to three facets. The inclination angles of these facets are categorized in two modes, defined either by periodic bond chains or by rows of atoms, each having two dangling bonds. Using the facet information, a simple atomic model is applied to the under-etch rates, based on removal frequencies of the chains or rows (f_p and f_k), and based on steps on flat {111} planes. Variations of under-etched surfaces sufficiently near to {111} planes are well-matched by the model. Planes near {110} and {100} cannot be matched by this simple formulation. Effective f_k increases more than f_p at low TMAH concentration. The etching of the same crystal planes can vary substantially at different geometrical attitudes under identical etchant conditions. For example, {110} surfaces are etched at several different rates in 12 wt% TMAH at 80°C.

1. Introduction

Etch rate anisotropy as a function of crystal orientation has been experimentally studied in various etchants for several decades by many authors (refs. 1–11, for example). Deep global minima are always observed at {111} planes. On the other hand, the etch rate variations of faster-etching planes differ from etchant to etchant and can depend sensitively on etchant, etchant concentration, temperature, and additives. While it is readily understood that the minima at {111} planes are due to the crystal bonding configuration (this is the only plane where each surface atom has three back bonds, dominating a single dangling bond), modeling the etch rate anisotropy for faster-etching planes has been difficult.

*Corresponding Author, e-mail address: leslie@ece.concordia.ca

This research employs an approach based on the relation of experimental observations of geometrical features to the underlying crystal structure. The aim is to identify ranges of data which obey simple atomic models, and ranges of data which require more complex modeling. Si{110} is studied due to the rich complexity of under-etched planes exposed during under-etch experiments. The analysis is supplemented by Si{100} experiments. Two concentrations of TMAH are presented, 25 wt% and 12 wt%, both at 80°C. Variations in under-etch rates and under-etched surface geometries with mask-edge orientation are analyzed according to a simple geometrical model in silicon based on periodic bond chains and rows of atoms, each having two dangling bonds. The data agree with the model in some ranges of the variable space and not in others, thereby providing a focus for more advanced modeling.

2. Atomic Model

For the sake of argument, the etch mechanism in silicon is modeled in this work by a small number of basic atomic structures: flat Si{111} planes, periodic bond chains[7,12] ("pbc's" —the building blocks of Si{110} planes), and rows of "kinks" (defined here as atoms, each having two dangling bonds free to interact with the etchant, and two back bonds[7,13] —theoretical Si{100} planes are fields of such features, with row and bond orientations alternating from one atomic layer to the next). Surface reconstruction is not considered, and the Si{111} plane is *assumed* to be the only inherently flat plane serving as a reference for the propagation of steps. The model assumes (again, for the sake of argument) that any etched surface can be interpreted as having indices of the form {hhk} or {hkk}, where h≥k. Any surface having indices {hhk} is composed of steps defined by pbc's, while any surface having indices {hkk} is composed of steps defined by regular rows of kinks. While these assumptions may not be true for all cases, they cover a wide enough set of data to make them useful.

In accordance with basic crystal growth and etch models, etching is simply modeled as the movement of steps. Figure 1(a) depicts an etching surface defined by steps on a flat plane. Assuming that, in a single unit of time ($1/f$), the etch propagates by one step-advancement width s (assumed to occur on each step simultaneously), the etch rate can be calculated as $ER(\theta) = s*f*\sin(\theta)$. The step height, r, represents the perpendicular spacing between {111} planes. The left-hand side of Fig. 1(b) depicts a typical pbc-defined {hhk} surface, while the right-hand side depicts a typical {hkk} "k-based" surface. For these two generic cases, the etch rates are as follows:

$$ER_p(\theta_p) = 3.31\text{Å}\, f_p \sin(\theta_p) \text{ and}$$
$$ER_k(\theta_k) = 3.31\text{Å}\, f_k \sin(\theta_k),$$

where f_p and f_k are the removal frequencies of pbc's and rows of kinks, respectively, and θ_p and θ_k are the angles between the {111} flat plane in question and the pbc-based or k-based plane being considered. The numerical values of the step width and height are taken to be the same for both pbc-defined and k-defined cases. These types of equations can only be

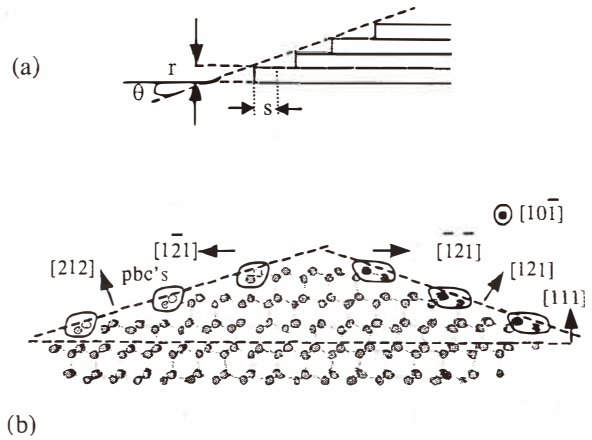

Fig. 1. Step-based model of etching; (a) an etching surface schematically depicted as defined by steps on flat planes; (b) etcing surfaces (left: defined by pbc's, right: defined by rows of kinks), depicted atomically as steps on flat {111} planes.

expected to hold within certain angle intervals close to the flat reference plane. For sufficiently large θ, interactions with other flat planes may dominate.

For a given silicon wafer surface, such as {110} or {100}, there are several distinguishable {111}-family planes, each of which can potentially serve as a flat plane, to which θ can be referenced.

The orientation of these {111} planes with respect to the wafer surface is of critical importance in interpreting etch behaviour. While the {100} surface presents four symmetric {111} planes, each inclined by 54.7° to the horizontal, the {110} surface presents vertical {111} planes in a parallelogram arrangement, and two 35.3° inclined {111} planes. Effectively, when etching Si{100}, there is only one main type of variation of (θ_p) and (θ_k). The inclination angles of pbc-based planes vary between 54.7° and 45°, while kink-based planes vary between 54.7° and 125.3° (inverted). On the other hand, for the etching of Si{110}, the situation is more complicated.

The relevant possibilities for wafers of both orientations are summarized in abbreviated form in Table 1. In the pair-variation identifier, the leading letter indicates the type of plane, the first number is the inclination angle of the flat {111} plane taken as reference for θ, the middle number is the inclination angle of first-reached {110} or {100} plane as θ varies, and the last number is the inclination angle of the next {111} plane which is reached as θ varies. As θ varies, the intersection line of the planes with the {110} or {100} wafer surface varies as well. This variation is described by the deviation angle (δ) which, on {110} wafers, is measured from the intersection of a 35.3°-inclined {111} plane with the wafer surface. On {100} wafers, δ is measured from the intersection of a 54.7°-inclined {111} plane with the wafer surface. Figure 1 depicts cases where the planes are all perpendicular to the wafer surface. In real cases, this is usually not true, and some geometrical transformations are needed. The step widths for use in the transformed undercetch rate equations are also provided in Table 1. Figure 2(a) gives the calculated theoretical

Table 1(a)
Relevant Si{110} etch-variation cases.

Pair-Variation Identifier	Dev-Angle (δ) Range	Step width(s) on {110} surface
P-35-60-90	0-35-55	3.83 Å
P-90-90-90	55-90-125	3.31 Å
K-35-45-90	0-90-125	3.83 Å
K-90-90-90	125-0-55	3.31 Å
P-145-120-90	0-35-55	3.83 Å
K-145-135-90	0-90-125	3.83 Å

Table 1(b)
Relevant Si{100} etch-variation cases.

Pair-Variation Identifier	Dev-Angle (δ) Range	Step width(s) on {100} surface
P-55-45-55	-45 – 0 - +45	3.83 Å
K-55-90-125	-45 – 0 - +45	3.83 Å

inclination angles of the model planes in the {110} system, for comparison with the experimental data, including inverted planes having inclination angles >90°. A similar graph can be readily constructed for the far less complicated case of {100} wafers.

3. Experiments and Results

Lightly doped p-type Si{110} and {100} wafers were cleaned, thermally oxidized, and patterned using a wagon-wheel[1,11] mask pattern with spokes every 1°. All etches were carried out at 80°C, unstirred, to a depth of 20–50 μm in differing concentrations of TMAH, 25 wt% or 12 wt%. For each etch, fresh 25 wt% TMAH was used, with or without dilution. The TMAH was purchased from Moses Lake Industries, Inc. Manassas, VA. All of the etches in this work were performed in an etch system consisting of a beaker immersed in a temperature-controlled oil bath. The TMAH temperature in the beaker was monitored throughout the experiment using a thermometer. The beaker was fitted with a reflux condenser cap to maintain the TMAH concentration at its nominal value. After etching, each sample was rinsed in deionized water, then methanol, and carefully dried by gently blowing nitrogen to avoid breaking the overhanging oxide. Finally, the under-etch distances and under-etched facet inclination angles were characterized in detail using a combination of optical microscopy and SEM.[11]

The under-etch results are shown in Figs. 2(b) to 2(e) for Si{110} and in Figs. 3(a) to 3(d) for Si{100}. In the case of 25 wt%, the {110} and {100} wafers were etched simultaneously in the same bath. Description of the under-etched surfaces was found to be quite complex, often involving two to three facets and varying roughnesses.[11] The facet inclination angles are estimated to within ±2° for smooth surfaces, with less accuracy for

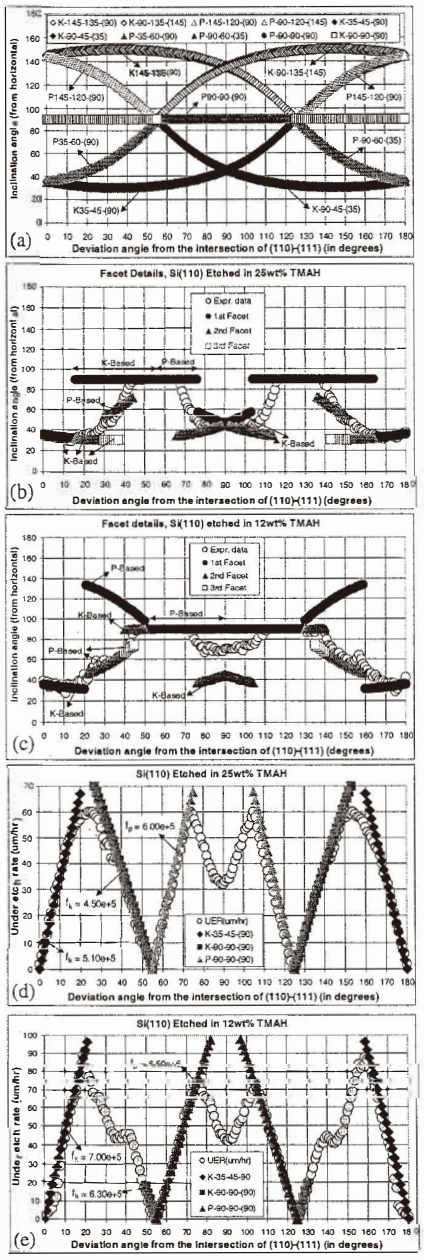

Fig. 2. For Si{110} (a) theoretical inclination angles (see Table 1 for pair-variation identifiers), (b,c) experimental facet information; (d,e) experimental *UER* curves, and fitted theoretical *UER* curves, with corresponding pbc- or k-row-removal frequencies. "Expr." data give the effective inclination angle, as if there were only one facet.

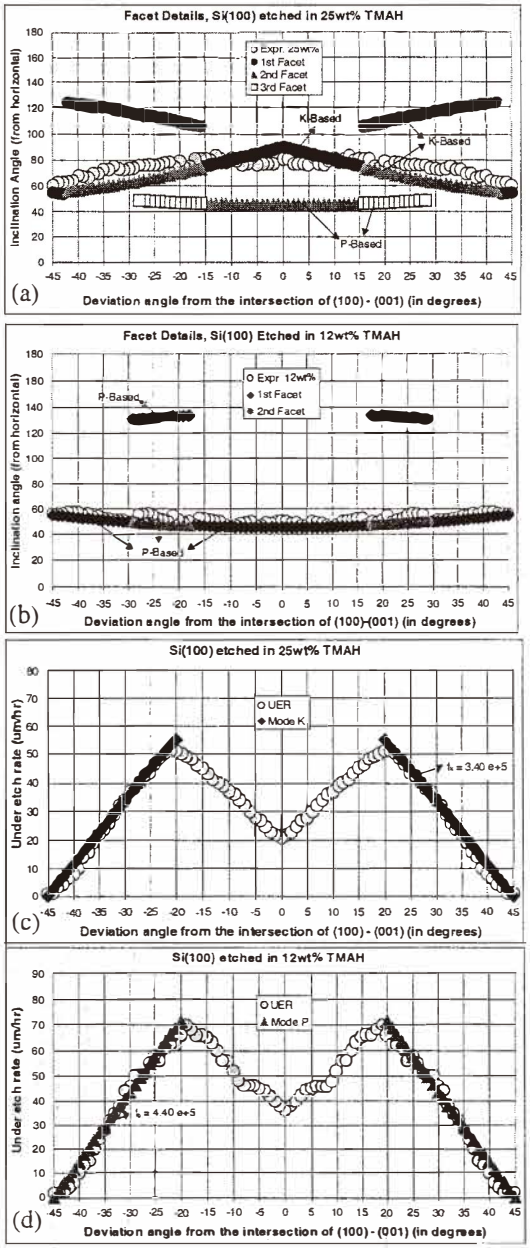

Fig. 3. For Si{100} (a,b) experimental facet information; (c,d) experimental *UER* curves, with corresponding pbc- or k-row-removal frequencies. "Expr." data give the effective inclination angle, as if there were only one facet.

rough surfaces. The under-etch rate ($UER(\delta_p$ or $\delta_k)$) is based on the under-etch distance, measured from the mask edge to where the top (first) facet intersects the horizontal wafer surface.

Figures 2(b) and 2(c) for {110} wafers show the facets of the under-etched surfaces, all at or near one of the theoretical plane variations outlined in Fig. 2(a). Data labeled as "Expr." give the effective inclination angles,[11] calculated as if there were only one facet. Figures 3(a) and 3(b) similarly show the facets of the under-etched surfaces on {100} wafers. Again, all of the facets are found to be at or near one of the theoretical pbc-based or k-row-based plane variations (not shown). Figs. 2(d) and 2(e) for {110} wafers and 3(c) and 3(d) for {100} wafers show the under-etch rates. This data, along with the facet inclination angles, allows direct fitting by the atomic model as described below.

4. Observations and Model Fitting

By comparing the experimental facet inclination angles in Figs. 2(b) and 2(c) (for {110} wafers) with the theoretical inclination angles in Fig. 2(a), one can readily identify k-based and p-based under-etched facets. If roughness is ignored, for the moment, each (all) of the under-etched surfaces can be assigned to one of the {hhk}- or {hkk}-based curves in Fig. 2(a). This result is very important, since it means that essentially all of the under-etched surfaces in these experimental cases are *at or near* crystal surfaces defined by k-based or p-based steps.

From this information in Figs. 2(b) and 2(c), the *UER* curves for Si{110} are fitted to the appropriate $UER(\delta_p)$ or $UER(\delta_k)$ in certain ranges, and the corresponding f_p and f_k values are calculated (in #/h). Fitted curves are overlaid on the under-etch data in Figs. 2(d) and 2(e), along with the corresponding pbc- and k-row-removal frequencies. Similarly, in the {100} case, the fitted curves are overlaid on the under-etch data in Figs. 3(c) and 3(d).

Consistent with trends reported in the literature for the etch rate of silicon in TMAH, f_p and f_k tend to be greater at the lower TMAH concentration. By direct comparison (only readily available in the {110} case), this work shows that the greater increase is in f_k (7e5 vs. 5.1e5), rather than in f_p (6.5e5 vs. 6e5).

It is also clear from our model-fitting efforts that the deviation-angle range between 75° and 105° in Si{110} and the deviation-angle range between –20° and +20° in Si{100} cannot be fitted by any such simple model where {111} planes are taken as the only flat reference plane. In these ranges, the under-etched planes are near to inclined {110} and/or {100} planes. Nonetheless, the etch rates of these planes, as found from the etch depths, exhibit a similar trend at lower TMAH concentration: the etch rate of the kink-based plane, {100}, increases dramatically, while the etch rate of the pbc-based plane, {110}, decreases slightly:

25 wt% {100}*ER*=24 μm/h
12 wt% {100}*ER*=37 μm/h
25 wt% {110}*ER*=44 μm/h
12 wt% {110}*ER*=40 μm/h

In a related vein, pbc-based {110} surfaces are etched at different rates in 12 wt% TMAH:

{110} horizontal wafer surface: (average) 40 μm/h

$\delta = 90°$ underetched {110} on {110} wafer: 42 μm/h

$\delta = 0°$ underetched {110} on {100} wafer: 29 μm/h

Similarly, kink-based {100} surfaces are etched at different rates in 25 wt% TMAH:

{100} horizontal wafer surface: (average) 24 μm/h

$\delta = 90°$ underetched {100} on {110} wafer: 23 μm/h

$\delta = 0°$ underetched {100} on {100} wafer: 21 μm/h.

Beyond the above reductions in etch rate near {100} and {110} planes, fits to the data on {100} silicon wafers (Figs. 3(c) and 3(d)), show that the k-row- and pbc-removal rates are significantly reduced during under-etch experiments on {100} wafers vs their {110} counterparts (f_k = 3.4e5 in 25 wt%, and f_p = 4.4e5 in 12 wt%). This further supports the observation that the etching of the same crystal planes (in identical etchant conditions) can vary substantially at different geometrical attitudes with respect to the mask. Note that in certain ranges of the data for Si{100}, the under-etch data was fitted to the second facets, since the inverted top-most facets were very small and could be accounted for by minor adjustments.

5. Conclusions

- Under-etching Si{110} provides rich variations of experimental data.
- Several under-etched facets often appear.
- Most facet inclination angles vary in one of two modes, corresponding to {hhk} or {hkk} step-based planes.
- The method allows the isolation of removal rates of pbc's and rows of atoms having two dangling bonds, to observe how they vary with experimental variables.
- f_k increases substantially at low TMAH concentration.
- f_p, and f_k appear to vary with position or geometry under constant etchant conditions.
- Effective removal rates are dramatically reduced near {110} and {100} planes, yet follow the same trend as low-θ removal rates.

Acknowledgements

This work was partially supported by funding from the Natural Sciences and Engineering Research Council of Canada (NSERC) and from the Fonds pour la Formation des Chercheurs et l'Aide a la Recherche (FCAR).

References

1 H. Seidel, L. Csepregi, A. Heuberger and H. Baumgartel: J. Electrochem. Soc. **137** (1990) 3612.

2 D. L. Kendall: J. Vac. Sci. & Technol. A **8** (1990) 3598.

3 O. Tabata, R. Asahi, H. Funabashi, K. Shimaoka and S. Sugiyama: *S*ensors and Actuators A **34** (1992) 51.

4 A. Merlos, M. Acero, M. H. Bao, J. Bausells and J. Esteve: Sensors and Actuators A **37–38** (1993) 737.
5 M. Elwenspoek, U. Lindberg, H. Kok and L. Smith: Proc IEEE-MEMS-1994, Oiso, Japan, p. 223.
6 S. S. Tan, M. L. Reed, H. Han and R. Boudreau: J. Microelectromech. Sys. **5** (1996) 66.
7 L. M. Landsberger, S. Naseh, M. Kahrizi, and M. Paranjape: J. Microelectromech. Sys. **5** (1996) 106.
8 O. Tabata: Proc. IEEE-MEMS-1998, Heidelberg, Germany, p. 229.
9 K. Sato, M. Shikida, T. Yamasiro, M. Tsunekawa and S. Ito: *in* Proc. IEEE-MEMS 1998, Heidelberg, Germany, p. 201
10 J. van Suchtelen, K. Sato, E. van Veenendaal, A. J. Nijdam, J. G. E. Gardeniers, W. J. P. van Enckevort, M. Elwenspoek: Proc. IEEE-MEMS-1999, Orlando, USA, p. 332.
11 A. Pandy, L. M. Landsberger and M. Kahrizi: Can. J. Elec. & Comp. Eng. **25** (2000) 19.
12 J. G. E. Gardeniers, W. E. J. R Maas, R. Z. C. Van Meerten, and L. J. Giling: J. Cryst. Growth **96** (1989) 832.
13 O. Than and S. Buttgenbach: Sensors and Actuators A **45** (1994) 85.